International Journal of Minerals, Metallurgy and Materials
Volume 25, Number 2, February 2018, Page 181
https://doi.org/10.1007/s12613-018-1561-3

Microstructural evolution of a superaustenitic stainless steel during a two-step deformation process

N. Bayat[1)], *G.R. Ebrahimi*[1)], *A. Momeni*[2)], *and H.R. Ezatpour*[3)]

1) Department of Materials and Polymer Engineering, Hakim Sabzevari University, Sabzevar 9617976487, Iran
2) Department of Materials Science and Engineering, Hamedan University of Technology, Hamedan 6516913733, Iran
3) Faculty of Engineering, Sabzevar University of New Technology, Sabzevar 9615918339, Iran
(Received: 10 April 2017; revised: 4 June 2017; accepted: 12 June 2017)

Abstract: Single- and two-step hot compression experiments were carried out on 16Cr25Ni6Mo superaustenitic stainless steel in the temperature range from 950 to 1150°C and at a strain rate of 0.1 s^{-1}. In the two-step tests, the first pass was interrupted at a strain of 0.2; after an interpass time of 5, 20, 40, 60, or 80 s, the test was resumed. The progress of dynamic recrystallization at the interruption strain was less than 10%. The static softening in the interpass period increased with increasing deformation temperature and increasing interpass time. The static recrystallization was found to be responsible for fast static softening in the temperature range from 950 to 1050°C. However, the gentle static softening at 1100 and 1150°C was attributed to the combination of static and metadynamic recrystallizations. The correlation between calculated fractional softening and microstructural observations showed that approximately 30% of interpass softening could be attributed to the static recovery. The microstructural observations illustrated the formation of fine recrystallized grains at the grain boundaries at longer interpass time. The Avrami kinetics equation was used to establish a relationship between the fractional softening and the interpass period. The activation energy for static softening was determined as 276 kJ/mol.

Keywords: superaustenitic stainless steel; dynamic recrystallization; static softening; metadynamic recrystallization; microstructural evolution; Avrami kinetics equation

1. Introduction

Microstructural evolutions during and after hot working of metallic materials strongly affect the final properties of the products. Dynamic recovery (DRV), dynamic recrystallization (DRX), static recovery (SRV), static recrystallization (SRX), and post-dynamic or metadynamic recrystallization (MDRX) are the most ubiquitous phenomena that can change the microstructure of metallic materials in a hot deformation process. These dynamic and static softening processes profoundly affect the microstructural evolution of metallic materials [1–2]. In low-stacking-fault-energy metals such as superaustenitic stainless steels, fine grains with very low dislocation density usually appear during deformation [3]. In this mechanism, primary grain boundaries elongate along the direction of applied stress. Afterwards, the grain boundaries bulge outward and form the primary volumes ready to crystallize. Recrystallization of new grains is activated when strain reaches a critical value defined as ε_c. This critical condition is often accompanied by the subgrains reaching a critical size [4]. The critical strain/condition is a function of the deformation condition as well as the primary microstructure. After this step, DRX proceeds via the occupation of prior grain boundaries by the new grains, forming what is referred to as a necklace structure [3,5]. The necklace microstructure has been observed in various materials deformed at small strains at elevated temperatures [6]. Temperature and strain rate have been reported to remarkably influence the necklace microstructure and the size of DRX grains [7–8]. By contrast, the effect of primary grain size has been negligible [9–10]. Despite numerous investigations devoted to this topic, no accurate mechanism that accounts for the formation of these types of grains, particularly the second layer of the necklace structure

Corresponding author: G.R. Ebrahimi E-mail: ebrahimi@hsu.ac.ir

has been proposed.

The presence of a massive density of dislocations in partially dynamic recrystallized microstructures results in a tendency toward post-deformation softening during the interpass period of a multistep hot working operation. When the pass strain is below the DRX critical strain, static recrystallization (SRX) is the major static softening process; when the pass strain is well above the critical strain, MDRX is the dominant static softening process [11–12].

The sensitivity of static restoration mechanisms to deformation parameters depends on the type of process [13]. When MDRX is the dominant interpass softening mechanism, softening kinetics are highly dependent on the strain rate, temperature, and the chemical composition of the metallic material [14]. In this condition, the pass strain and the initial grain size are not considered as effective factors [15–18]. By contrast, SRX is the most significant mechanism after low-pass strains; its kinetics is directly related to temperature, pass strain, and initial grain size, whereas it is weakly dependent on strain rate [13,19]. Therefore, a transition strain (ε^*) is defined as the strain point where softening behavior of the materials changes from a strain-dependent state at low strains to a strain-independent state at high strains. The transition strain is intermediate between the peak and the steady-state strains [20–21].

Despite numerous studies related to SRX and MDRX [22–26], the softening mechanisms in superaustenitic stainless steels remain poorly understood. Some interesting issues in this field are grain size changes during MDRX, the relation of these changes to the extent of softening, and the relationship between the fractions of DRX and MDRX.

In this study, single and two-step hot compression tests were performed on 16Cr25Ni6Mo superaustenitic stainless steel in the temperature range from 950 to 1150°C and at a strain rate of 0.1 s^{-1}. Mechanical and microstructural examinations were used to investigate the static softening behavior of the material during the interpass period.

2. Experimental

The chemical composition of the superaustenitic stainless steel 16Cr25Ni6Mo used in this study is presented in Table 1. The initial microstructure of the material exhibited in Fig. 1 shows a fully recrystallized structure of equiaxed grains with an average grain size of 150 μm. The average grain size was determined by the intercept method described in standard ASTM E112.

Table 1. Chemical composition of the 16Cr25Ni6Mo steel (Fe balance) used in this work wt%

C	Si	Mn	Cr	Mo	Ni	Nb	Al	Cu	Co	V	W	N
0.052	0.48	1.472	18.91	6.23	23.78	0.044	0.23	0.15	0.103	0.7	0.239	0.571

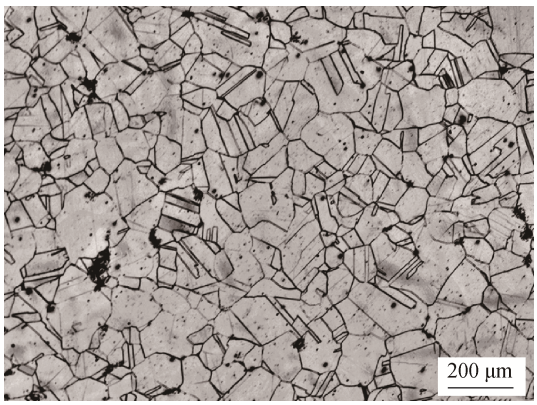

Fig. 1. Initial microstructure of the used material.

Hot compression tests were performed using a Zwick-Roell 250 universal testing machine. A resistance furnace was used to control the deformation temperature with a precision of ±5°C. Samples with a diameter and a height of 8 and 12 mm, respectively, were prepared according to standard ASTM E209.

Schematics of the single- and double-hit compression tests adopted in this work are shown in Fig. 2. Before each test, a specimen was heated at 10°C/s to 1200°C and maintained at this temperature for 5 min. The reheated samples were cooled to the deformation temperature, where they were maintained for 3 min to eliminate any temperature gradient, and were then subjected to hot compression.

To investigate the flow curves, the single-hit hot compression tests were carried out in the temperature range from 950 to 1150°C at intervals of 50°C and with a constant strain rate of 0.1 s^{-1}. With regard to the critical and peak strains, a strain of 0.2 was selected as the interrupting strain of the first pass in the double-hit tests. The kinetics of static softening mechanisms was investigated within various interpass times of 5, 20, 40, 60, and 80 s. After a total strain of 0.7, the deformed samples were quenched in water to ambient temperature. To study the microstructures after the interpass period, some samples were deformed in the first pass, held for different interpass times of 5, 20, 40, 60, and 80 s, and then quenched to room temperature. Optical microscopy

observations were carried out to determine the extent of static softening during the interpass period.

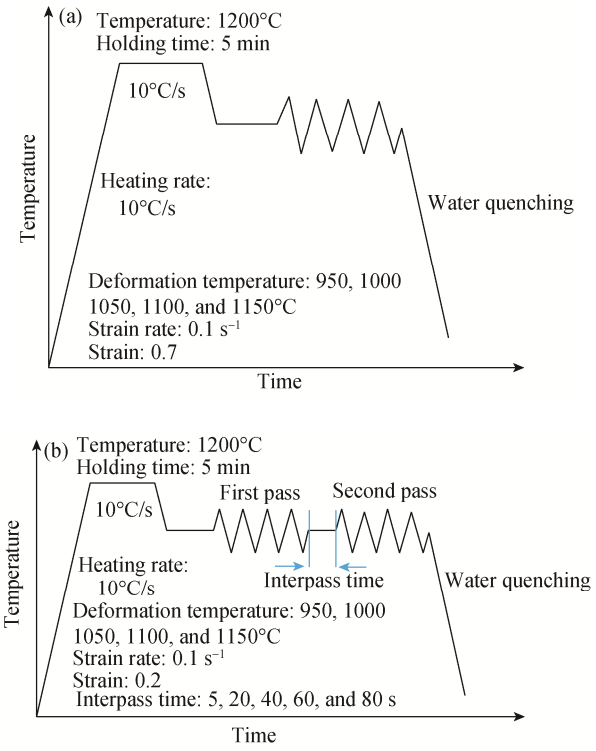

Fig. 2. Schematic of the thermomechanical processes applied to the samples: (a) one-step deformation; (b) two-step deformation.

3. Results and discussion

3.1. Single-hit flow curves and microstructures

The true stress–strain curves of the material in the temperature range from 950 to 1150°C and corresponding to a strain rate of 0.1 s^{-1} are shown in Fig. 3. All the curves exhibit a peak that indicates the occurrence of DRX. Accordingly, the values of both the peak strain and the peak stress increase with decreasing temperature.

The critical and peak strains (ε_c and ε_p) and the critical and peak stresses (σ_c and σ_p) are often determined from a plot of the work-hardening rate (θ) vs. the flow stress. In this method [27–28], σ_p is identified as the point where the work-hardening slope reaches zero. As evident in Fig. 4, three inflections are observed in the θ–σ plots; these inflections correspond to the substructure formation, the critical point, and the peak point. The values of ε_c, ε_p, σ_c, and σ_p determined by the aforementioned method are summarized in Table 2.

Similarly, the points corresponding to the highest rate of DRX and the onset of the steady-state condition are easily distinguished in a plot of θ vs. true strain. As shown in Fig. 5, θ becomes negative in the DRX region and reaches a minimum at $\varepsilon = \varepsilon^* = \varepsilon_{50\%}$, which refers to the highest rate of DRX. The θ then increases again and reaches zero at $\varepsilon = \varepsilon_{ss}$, which is known as the onset of the steady-state region. Table 3 summarizes the ε^* and ε_{ss} values at different temperatures.

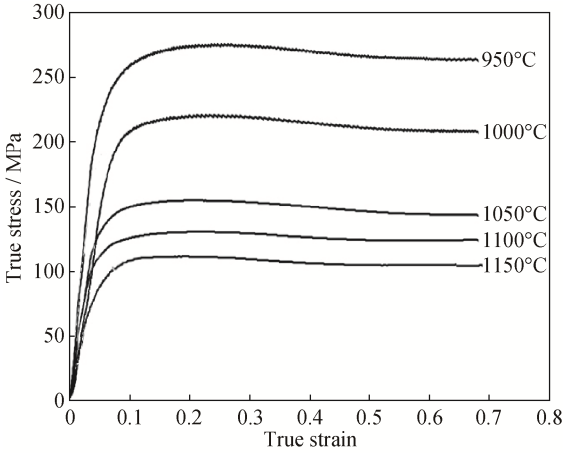

Fig. 3. Stress–strain curves at different temperatures and a final strain of 0.7.

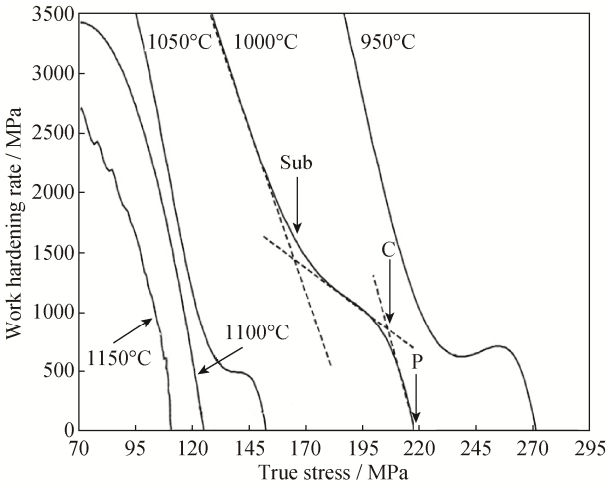

Fig. 4. Work-hardening rate versus true stress at various deformation temperatures. The points corresponding to the formation of substructure, initiation of DRX (critical point), and the peak are highlighted at 1000°C.

Table 2. Peak and critical stress and strain at different deformation temperatures

Temperature / °C	σ_p / MPa	ε_p	σ_c / MPa	ε_c
950	274	0.218	258	0.140
1000	220	0.215	205	0.093
1050	154	0.176	145	0.080
1100	130	0.165	93	0.031
1150	128	0.160	89	0.028

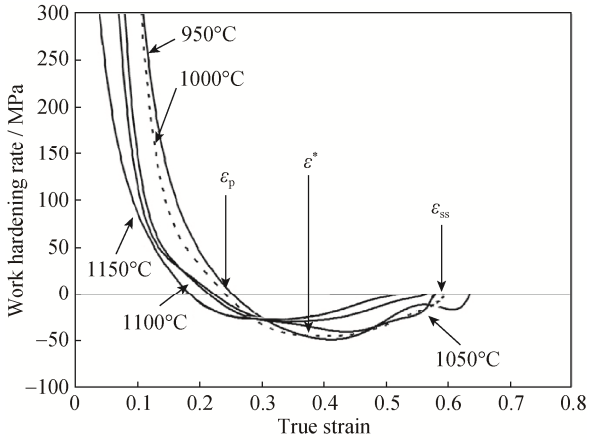

Fig. 5. Work-hardening rate versus true strain at various deformation temperatures. The points corresponding to 50% DRX ($\varepsilon = \varepsilon^* = \varepsilon_{50\%}$) and the onset of the steady-state region (ε_{ss}) are highlighted at 1000°C.

Table 3. Values of strain corresponding to 50% DRX and onset of the steady-state region at various deformation temperatures

Temperature / °C	$\varepsilon_{50\%}$ (ε^*)	ε_{ss}
950	0.42	0.63
1000	0.38	0.60
1050	0.33	0.55
1100	0.30	0.50
1150	0.28	0.45

The results in Tables 2 and 3 show that, under all of the studied deformation conditions, DRX starts at strains of approximately 0.2. The progression of DRX at the peak is often limited to approximately 10%; the rest of the microstructure remains in the deformed condition [29]. This result is clearly comprehended from the $\varepsilon_p/\varepsilon_{50\%}$ ratio, which is less than 0.5. Therefore, if the deformation is interrupted at a strain of 0.2, the microstructure mainly consists of deformed grains ready to be statically recrystallized by heating in the interpass period. In the interpass period, the work-hardened part of the structure is softened by SRX. However, concomitant with the SRX in the work-hardened grains, MDRX occurs in the small regions that had experienced DRX in the first pass. That is, SRX is prevalent at approximately 90% of the microstructure, whereas MDRX occurs in the other 10% of the microstructure. The micrographs in Fig. 6 confirm that, at the peak, DRX has progressed only slightly, especially at temperatures below 1100°C, and is enclosed in the formation of bulges and a few small grains along the grain boundaries. The elongated grains contain a large amount of stored deformation energy, which enables them to undergo SRX in the interpass period. During the interpass period, fine SRX grains are formed in the deformed regions, rapidly consuming the stored energy. However, the low energy content of small DRX grains leads to limited softening by MDRX. On this basis, SRX is the major static softening mechanism for a material deformed to a strain of 0.2 in the first pass.

3.2. Double-hit flow curves and microstructures

Fig. 7 presents the flow curves corresponding to double-hit compression tests carried out at various tempera tures with different interpass times of 5, 20, 40, 60, and 80 s. The flow stress level in the second pass decreases, especially

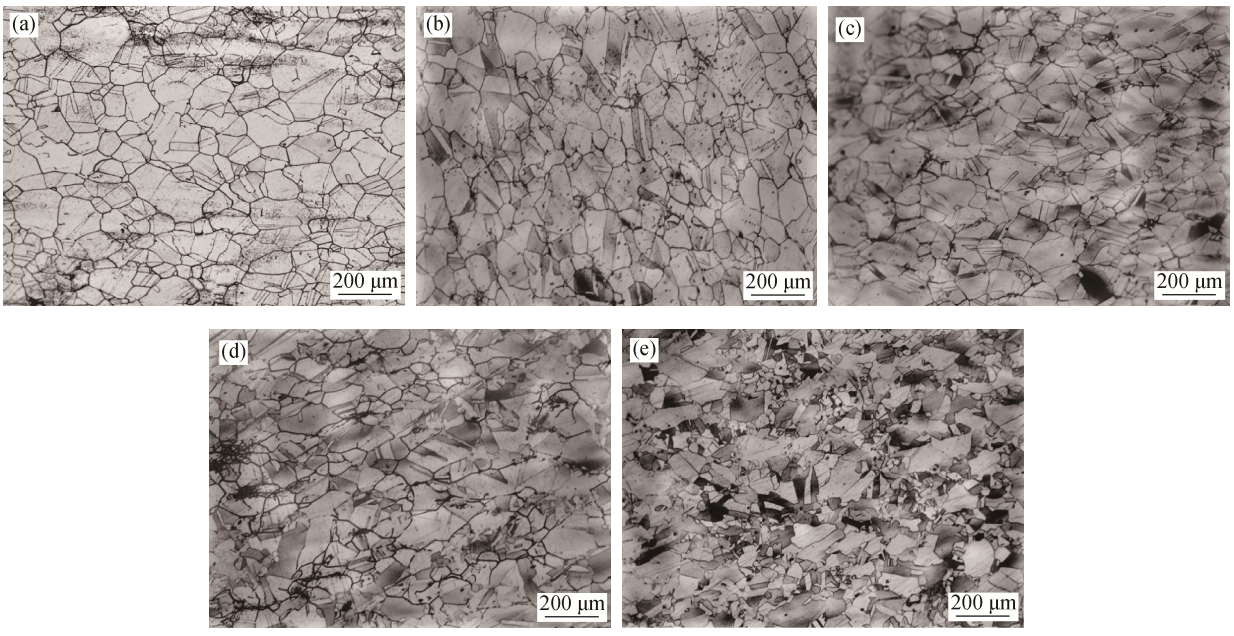

Fig. 6. Micrographs of the samples deformed up to the peak at 950°C (a), 1000°C (b), 1050°C (c), 1100°C (d), and 1150°C (e).

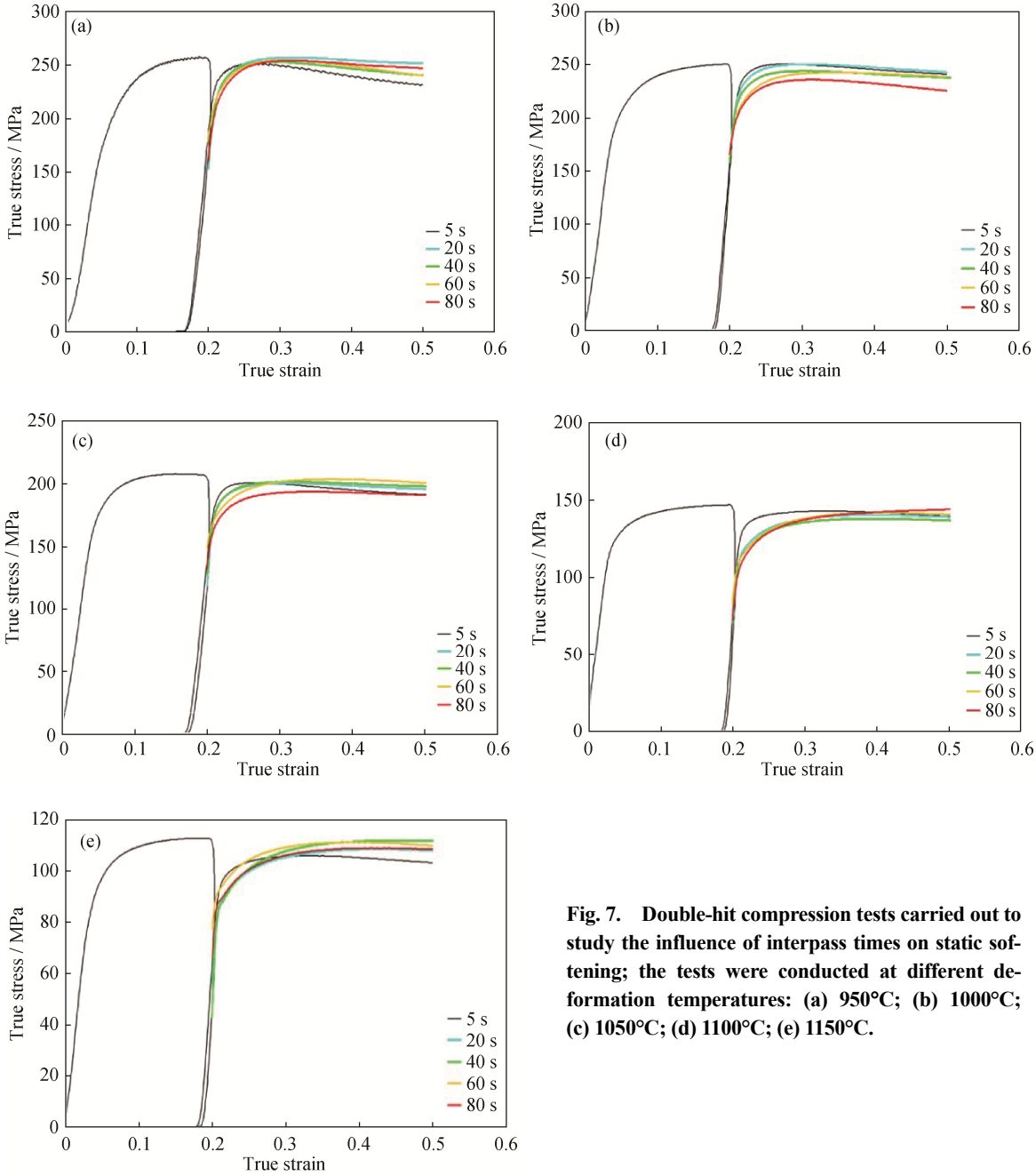

Fig. 7. Double-hit compression tests carried out to study the influence of interpass times on static softening; the tests were conducted at different deformation temperatures: (a) 950°C; (b) 1000°C; (c) 1050°C; (d) 1100°C; (e) 1150°C.

after longer interpass times. As previously mentioned, the interpass softening is attributable to SRX in the deformed grains and MDRX in the dynamically recrystallized parts of the structure.

The interpass softening is evaluated using the following equation [30]:

$$X = \frac{\sigma_m - \sigma_2}{\sigma_m - \sigma_1} \quad (1)$$

where X is the static fractional softening, which varies between 0 and 1, σ_m is the flow stress at the end of the first pass (interrupted stress), and σ_1 and σ_2 refer to the yield stresses of the first and second passes, respectively. With longer interpass times and greater progression of interpass softening, σ_2 decreases, leading to an increase of X. That is, with increasing interpass time, $\sigma_m - \sigma_2$ increases and X therefore increases between 0 and 1. Fig. 8 shows the variation of X with the interpass time at various deformation temperatures. As clearly shown, the fractional softening increases from approximately 0.27 after 5 s of holding at 950°C to nearly 1 after an interpass time of 80 s at 1150°C. The increase of X at higher temperatures is associated with the promotion of SRX and MDRX. Notably, the distance

between curves in Fig. 8 decreases with increasing temperature. Thus, at a given interpass time, an increase in temperature within the range from 950 to 1050°C results in a more remarkable increase in the value of X compared with its increase in the higher-temperature range from 1100 to 1150°C. This result suggests different static softening mechanisms at temperatures greater than and less than 1050°C. According to Fig. 6, at the end of the first pass in the temperature range from 950 to 1050°C, no DRX grains were observed in the microstructure. However, at 1100 and 1150°C, small DRX grains were observed near the prior grain boundaries. Therefore, although the static softening at 950–1050°C involves only SRX in the deformed grains, at 1100 and 1150°C, it involves SRX in the deformed areas and MDRX in the small DRX grains. Notably, when partial DRX occurs during the first pass, it consumes some of the strain energy and therefore decelerates the kinetics of subsequent static softening.

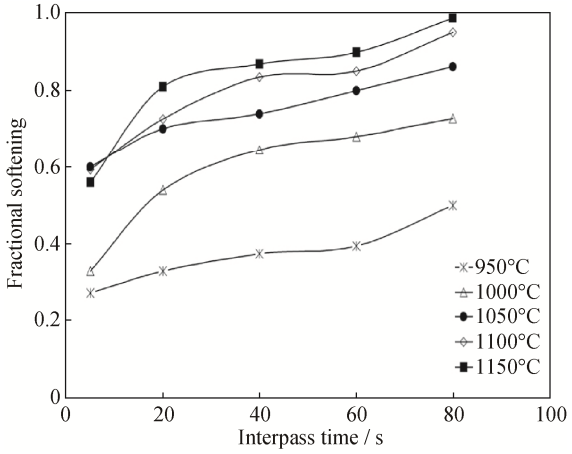

Fig. 8. Fractional softening (X) as a function of interpass time, calculated at various temperatures using Eq. (1).

Fig. 7 shows that the apparent features of the flow curves vary with the change in the interpass period. At all temperatures, the flow curve of the second pass is characterized by a distinct peak and remarkable flow softening after the interpass time of 5 s. However, after the holding times of 20 and 40 s, a weak peak is observed, followed by weak flow softening. A further increase in holding time to 60 and 80 s leads to a faint peak, after which a steady-state flow behavior is observed. Fig. 9 indicates that the ε_p for the second pass increases with increasing interpass time. All of these results imply that longer holding times degrade the tendency toward DRX in the second pass. When the interpass time is short, e.g., 5 s, SRX does not progress considerably and the dominant softening mechanism is SRV; consequently, the strain energy of the first pass remains after the interpass period and accumulates with the strain energy of the second pass. This accumulation, in turn, helps the material attain the critical condition for DRX at a lower ε_p. Less likely, after longer interpass times, SRX progresses, consumes the accumulated strain of the first pass, and shifts the ε_p toward larger strains.

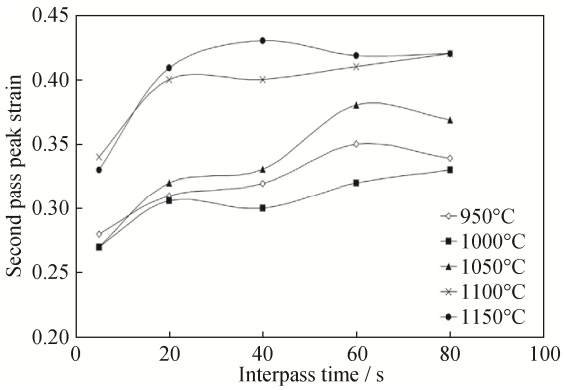

Fig. 9. Variation of the peak strain for the second pass with the interpass time.

Fig. 10 shows the representative micrographs of the samples after different interpass times. Fig. 10(a) shows that a 5-s holding time at 950°C is insufficient to initiate SRX in the elongated grains and that SRV is the only interpass softening mechanism. Therefore, the strain of the first pass is almost entirely accumulated and leads to fast DRX during the second pass. On the basis of the fractional softening results in Fig. 8, we deduced that SRV is responsible for approximately 0% of the static softening. This finding is consistent with the results of previous reports [24]. When the holding time is increased to 20 s (Fig. 10(b)), primary nuclei of SRX (indicated by arrows) nucleate around the grain boundaries and then grow during longer holding times such as 80 s (Fig. 10(c)).

At 1050°C, SRX initiates after 5 s (Fig. 10(d)) and occupies the prior austenite grain boundaries after 20 s (Fig. 10(e)). According to Fig. 8, the holding time of 80 s at 1050°C results in increased fractional softening to approximately 0.8, which is equal to 50% SRX, as shown in Fig. 10(e). When the deformation temperature is increased to 1150°C, the rate of static softening increases, leading to an increase in fractional softening to approximately 1 after the interpass time of 80 s. The grain size measurements summarized in Fig. 11 indicate that SRX substantially refines the final grain size. The results also indicate that increasing the temperature to 1050°C promotes SRX and leads to grain refinement. However, further temperature increases to 1100 and 1150°C result in fast grain growth. Therefore, the temperature of 1050°C is the optimum temperature to obtain the finest grain structure in the hot deformed material.

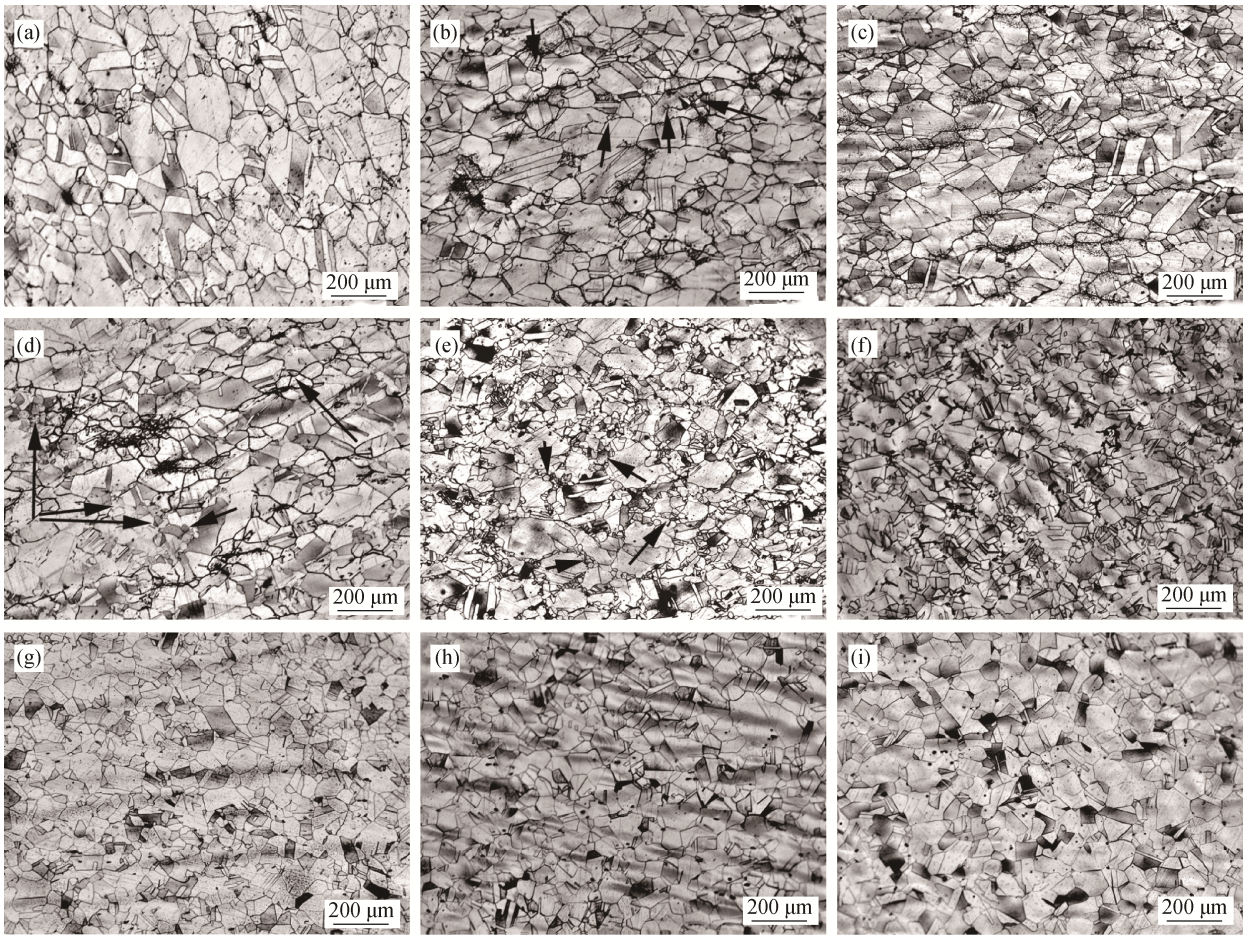

Fig. 10. Micrographs of the witness samples that conveyed the first pass of deformation up to a strain of 0.2 and at various interpass times: (a) 950°C, 5 s; (b) 950°C, 20 s; (c) 950°C, 80 s; (d) 1050°C, 5 s; (e) 1050°C, 20 s; (f) 1050°C, 80 s; (g) 1150°C, 5 s; (h) 1150°C, 20 s; (i) 1150°C, 80 s.

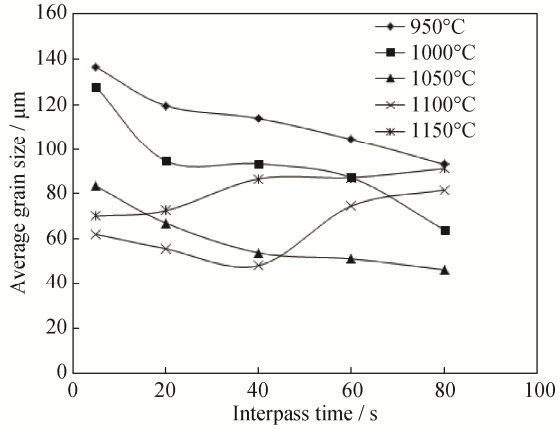

Fig. 11. Average grain size as a function of deformation temperature and interpass time.

The results also show that, at temperatures greater than 1050°C, an increase in the interpass time leads to an increase in the average grain size because of grain growth. However, at 950°C, a lower grain growth rate and a delay in the start of SRX lead to grain refinement at longer holding times.

3.3. Static softening kinetics

The kinetics of static softening after hot working is often described by the Avrami equation, given by [31]

$$X = 1 - \exp\left[-B\left(\frac{t}{t_f}\right)\right]^n \tag{2}$$

where X is the softening fraction, t and t_f are the interpass time and the interpass time for a specific value of softening equal to f, respectively, and n denotes the Avrami exponential constant. Parameter B is defined as

$$B = \ln(1 - f) \tag{3}$$

Generally, f is considered to be equal to 0.5. Hence, t_f would be equal to $t_{0.5}$ and B is determined to be 0.693. By substituting these values into Eq. (2), we obtain the following equation:

$$X = 1 - \exp\left[-0.693\left(\frac{t}{t_{0.5}}\right)\right]^n \tag{4}$$

Taking the logarithm of both sides of Eq. (4) gives

$$\ln\left[\ln\left(\frac{1}{1-X}\right)\right] = \ln 0.693 - n\ln t_{0.5} + n\ln t \tag{5}$$

In the plot of $\ln\{\ln[1/(1-X)]\}$ vs. $\ln t$, which should be a linear curve, the slope is equal to n and the intercept gives $\ln 0.693 - n\ln t_{0.5}$. As shown in Fig. 12, by plotting the experimental values according to Eq. (5), the average value of n is determined as 0.38. This value is smaller than those reported for other types of steels, which range from 0.8 to 1.3 [23]. This discrepancy is attributable to the low strain value adopted in this research. The rate of static softening and the value of n directly depend on the strain applied in the first pass of deformation. Therefore, the value of n would increase if larger strain was applied.

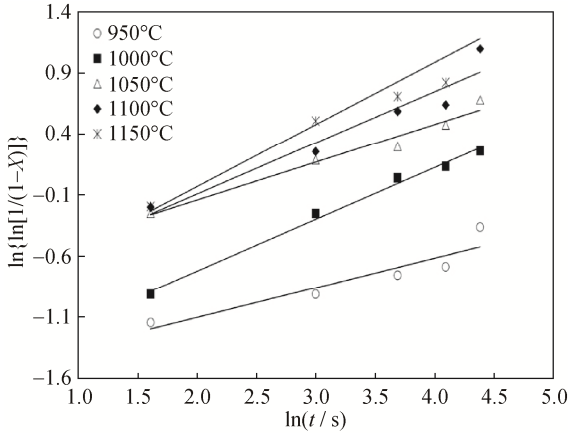

Fig. 12. Variation of fractional softening with interpass time in the framework of the Avrami kinetics equation (Eq. (5)).

The value of $t_{0.5}$ is an index of the rate of SRX and, according to the following equation, depends on the processing variables such as strain, temperature, and strain rate [31]:

$$t_{0.5} = A\varepsilon^{p}\dot{\varepsilon}^{q}\exp\left(\frac{Q_s}{RT}\right) \quad (6)$$

where A, p, and q are constants; T is the absolute temperature; Q_s is the activation energy for static softening (J/mol); and R is the universal gas constant (R = 8.314 J/(mol·K)).

Because the value of Q_s is an index to the easiness of static softening in a given material, it can be used to identify the rate-controlling sub-mechanism in static softening. On the basis of Eq. (6), the value of Q_s/R can be calculated by plotting the experimental data of $t_{0.5}$ versus the reciprocal of temperature on a logarithmic scale. According to the linear regression of experimental data in Fig. 13, the Q_s value is obtained as 276 kJ/mol. This value is in agreement with the values reported for SRX in other stainless steels [32–33] and reflects that the kinetics of static softening in this material is highly temperature sensitive [34].

4. Conclusions

Dynamic and static softening behaviors in 16Cr25Ni6Mo superaustenitic stainless steel were investigated through hot compression experiments in the temperature range from 950 to 1150°C and at a strain rate of 0.1 s^{-1}. The major achievements of this research are summarized as follows.

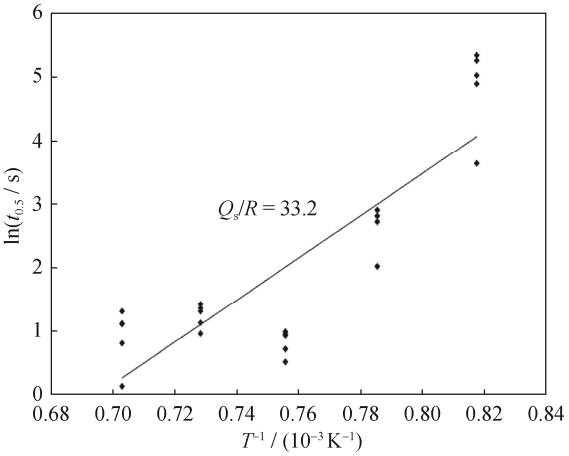

Fig. 13. Variation of ln $t_{0.5}$ with the reciprocal of temperature. The slope is equal to Q_s/R according to Eq. (6).

(1) Single-peak hot compression tests showed that, at temperatures from 950 to 1100°C, dynamic recrystallization exhibits no remarkable progress up to the peak point of the flow curves (ε = 0.2). At 1150°C, approximately 10% progress of dynamic recrystallization was observed in the form of new small grains at grain boundaries.

(2) The static softening ratio increased with increasing deformation temperature and interpass time. The fractional softening, which was approximately 0.27 after an interpass time of 5 s at 950°C, increased to approximately 1 at 1150°C and an interpass time of 80 s.

(3) At a given interpass time, the fractional softening increased with increasing temperature. The increase in fractional softening was remarkable up to 1050°C and gentle at 1100 and 1150°C. These results were attributed to the static softening at lower temperatures and to a combination of static and metadynamic recrystallizations at higher temperatures.

(4) The fractional softening and microstructural observations showed that approximately 30% of softening could be attributed to the static recovery.

(5) The Avrami kinetics equation was used to establish the relationship between the static fractional softening and the interpass period. The Avrami exponent and the activation energy for static softening were determined as 0.38 and 276 kJ/mol, respectively.

References

[1] M.S. Chen, K.K. Li, Y.C. Lin, and W.Q. Yuan, An improved

kinetics model to describe dynamic recrystallization behavior under inconstant deformation conditions, *J. Mater. Res.*, 31(2016), No. 19, p. 2994.

[2] M.Y. Li, Y.Z. Liu, T. Zhu, and Y. Wang, Microstructure homogenization control of Nb-bearing X65 pipeline steel by the CSP process, *Int. J. Miner. Metall. Mater.*, 18(2011), No. 1, p. 35.

[3] A. Momeni, G.R. Ebrahimi, M. Jahazi, and P. Bocher, Microstructure evolution at the onset of discontinuous dynamic recrystallization: A physics-based model of subgrain critical size, *J. Alloys Compd.*, 587(2014), p. 199.

[4] F.J. Humphrey and M. Hatherly, *Recrystallization and Related Annealing Phenomena*, 2nd ed., Oxford, 2004, p. 255.

[5] D. Ponge and G. Gottstein, Necklace formation during dynamic recrystallization: mechanisms and impact on flow behavior, *Acta Mater.*, 46(1998), No. 1, p. 69.

[6] G. Gottstein, E. Brunger, and D. Ponge, *Advances in Hot Deformation Textures and Microstructures*, TMS, Pennsylvania, l995, p. 477.

[7] A. Momeni, S.M. Abbasi, M. Morakabati, H. Badri, and X. Wang, Dynamic recrystallization behavior and constitutive analysis of Incoloy 901 under hot working condition, *Mater. Sci. Eng. A*, 615(2014), p. 51

[8] M. Ueki, S. Horie, and T. Nakamura, Factors affecting dynamic recrystallization of metals and alloys, *Mater. Sci. Technol.*, 3(1987), No. 5, p. 329.

[9] T. Sakai and J.J. Jonas, Dynamic recrystallization: Mechanical and microstructural considerations, *Acta Metall.*, 32(1984), No. 2, p. 189.

[10] A. Belyakov, H. Miura, and T. Sakai, Dynamic recrystallization in ultra fine-grained 304 stainless steel, *Scripta Metall.*, 43(2000), No. 1, p. 21.

[11] D.G. He, Y.C. Lin, M.S. Chen, and L. Li, Kinetics equations and microstructural evolution during metadynamic recrystallization in a nickel-based superalloy with δ phase, *J. Alloys Compd.*, 690(2017), p. 971.

[12] H.J. Mao, R. Zhang, L. Hua, and F. Yin, Study of static recrystallization behaviors of GCr15 steel under two-pass hot compression deformation, *J. Mater. Eng. Perform.*, 24(2015), No. 2, p. 930.

[13] B. Ma, Y. Peng, Y.F. Liu, and B. Jia, Modeling of metadynamic recrystallization kinetics after hot deformation of low-alloy steel Q345B, *J. Cent. South Univ. Technol.*, 17(2010), No. 5, p. 911.

[14] A. Dehghan-Manshadi, M.R. Barnett, and P.D. Hodgson, Hot deformation and recrystallization of austenitic stainless steel: Part I. Dynamic recrystallization, *Metall. Mater. Trans. A*, 39(2008), No. 6, p. 1359.

[15] A.R. Morgridge, Metadynamic recrystallization in C steels, *Bull. Mater. Sci.*, 25(2002), No. 4, p. 291.

[16] P.D. Hodgson, *Mathematical Modelling of Recrystallization Processes During the Hot Rolling of Steel* [Dissertation], University of Queensland, Brisbane, 1993.

[17] C. Roucoules, P.D. Hodgson, S. Yue, and J.J. Jonas, Softening and microstructural change following the dynamic recrystallization of austenite, *Metall. Mater. Trans. A*, 25(1994), No. 2, p. 389.

[18] W.P. Sun and E.B. Hawbolt, Comparison between static and metadynamic recrystallization—an application to the hot rolling of steels, *ISIJ Int.*, 37(1997), No. 10, p. 1000.

[19] A.M. Elwazri, P. Wanjara, and S. Yue, Metadynamic and static recrystallization of hypereutectoid steel, *ISIJ Int.*, 43(2003), No. 7, p. 1080.

[20] L.P. Karjalainen, T.M. Maccagno, and J.J. Jonas, Softening and flow stress behaviour of Nb microalloyed steels during hot rolling simulation, *ISIJ Int.*, 35(1995), No. 12, p. 1523.

[21] J.J. Jonas, The hot strip mill as an experimental tool, *ISIJ Int.*, 40(2000), No. 8, p. 731.

[22] B. Derby and M.F. Ashby, On dynamic recrystallization, *Scripta Metall.*, 21(1987), p. 879.

[23] A. Dehghan-Manshadi, H. Beladi, and M.R. Barnett, Recrystallization in 304 austenitic stainless steel, *Mater. Sci. Forum*, 467-470(2004), p. 1163.

[24] A. Dehghan Manshadi, *The Evolution of Recrystallization During and Following Hot Deformation* [Dissertation], Deakin University Geelong, Victoria, 2007.

[25] S. Venugopal, S.L. Mannan, and Y.V.R.K. Prasad, Processing maps for hot working of commercial grade wrought stainless steel type AISI 304, *Mater. Sci. Eng. A*, 177(1994), No. 1-2, p. 143.

[26] I. Salvatori, T. Inoue, and K. Nagai, Ultrafine grain structure through dynamic recrystallization for Type 304 stainless steel, *ISIJ Int.*, 42(2002), No. 7, p. 744.

[27] E.I. Poliak and J.J. Jonas, A one-parameter approach to determining the critical conditions for the initiation of dynamic recrystallization, *Acta Mater.*, 44(1996), No. 1, p. 127.

[28] G.R. Ebrahimi, H. Keshmiri, A.R. Maldad, and A. Momeni, Dynamic recrystallization behavior of 13%Cr martensitic stainless steel under hot working condition, *J. Mater. Sci. Technol.*, 28(2012), No. 5, p. 467.

[29] A. Momeni, S.M. Abbasi, and A. Shokuhfar, Dynamic and metadynamic recrystallization of a martensitic precipitation hardenable stainless steel, *Can. Metall. Q.*, 46(2007), No. 2, p. 189.

[30] A. Najafizadeh, J.J. Jonas, G.R. Stewart, and E.I. Poliak, The strain dependence of postdynamic recrystallization in 304 H stainless steel, *Metall. Mater. Trans. A*, 37(2006), No. 6, p. 1899.

[31] J. Liu, Y.G. Liu, H. Lin, and M.Q. Li, The metadynamic recrystallization in the two-stage isothermal compression of 300M steel, *Mater. Sci. Eng. A*, 565(2013), p. 126.

[32] X.W. Duan, M.M. Chen, H.Q. Chen, and J.S. Liu, Study on static recrystallization softening behavior of 316LN steel, [in] *Third International Conference on Measuring Technology and Mechatronics Automation (ICMTMA)*, 2011, Washington, p. 522.

[33] J. Liu, G.W. Fan, P.D. Han, J.F. Yang, J.S. Liu, D.S. Ge, and G.J. Qiao, Study on the static recrystallization behavior of thermal deformation of austenitic stainless steel for nuclear power, *Mater. Sci. Forum*, 658(2010), p. 165.

[34] H.Y. Wu, L.X. Du, Z.R. Ai, and X.H. Liu, Static recrystallization and precipitation behavior of a weathering steel microalloyed with vanadium, *J. Mater. Sci. Technol.*, 29(2013), No. 12, p. 1197.